

Discovery of the 198 s X-ray Pulsar GRO J2058+42

Colleen A. Wilson, Mark H. Finger¹, B. Alan Harmon
ES 84 Space Sciences Laboratory, NASA/Marshall Space Flight Center, Huntsville, AL 35812;
wilsonc@gibson.msfc.nasa.gov, finger@gibson.msfc.nasa.gov, harmon@ssl.msfc.nasa.gov

Deepto Chakrabarty
Center for Space Research, Massachusetts Institute of Technology, Cambridge, MA 02139;
deepto@space.mit.edu

and

Tod Strohmayer
Universities Space Research Association, Laboratory for High Energy Astrophysics, NASA/Goddard Space
Flight Center, Greenbelt, MD 20771; stroh@pcasrv1.gsfc.nasa.gov

ABSTRACT

GRO J2058+42, a transient 198 second x-ray pulsar, was discovered by the Burst and Transient Source Experiment (BATSE) on the *Compton Gamma-Ray Observatory (CGRO)*, during a “giant” outburst in 1995 September-October. The total flux peaked at about 300 mCrab (20-50 keV) as measured by Earth occultation. The pulse period decreased from 198 s to 196 s during the 46-day outburst. The pulse shape evolved over the course of the outburst and exhibited energy dependent variations. BATSE observed five additional weak outbursts from GRO J2058+42, each with two week duration and peak pulsed flux of about 15 mCrab (20-50 keV), that were spaced by about 110 days. An observation of the 1996 November outburst by the *Rossi X-ray Timing Explorer (RXTE)* Proportional Counter Array (PCA) localized the source to within a 4' radius error circle (90% confidence) centered on R.A. = 20^h 59^m.0, Decl. = 41°43' (J2000). Additional shorter outbursts with peak pulsed fluxes of about 8 mCrab were detected by BATSE halfway between the first four 15 mCrab outbursts. The *RXTE* All-Sky Monitor detected all 8 weak outbursts with approximately equal durations and intensities. GRO J2058+42 is most likely a Be/X-ray binary that appears to outburst at periastron and apastron. No optical counterpart has been identified to date and no x-ray source was present in the error circle in archival *ROSAT* observations.

Subject headings: pulsars: individual: GRO J2058+42 — stars: neutron — X-rays: stars — binaries: X-ray

¹*CGRO* Science Support Center/ Goddard Space Flight Center

1. Introduction

In the last 25 years more than 40 accretion-powered x-ray pulsars have been detected. About half of these are transient, of which 12 have known Be star companions. Neutron stars with Be companions accrete material from the slow, dense, stellar outflow thought to be confined to the equatorial plane of the Be star. Recent long term studies by the Burst and Transient Source Experiment (BATSE) on the *Compton Gamma-Ray Observatory* (*CGRO*) revealed that Be/X-ray binaries exhibit series of often periodic outbursts. These outbursts are sometimes associated with “giant” outbursts accompanied by high spin-up rates and luminosities. BATSE observed four additional accreting x-ray pulsars, without identified companions, which are believed to also be Be/X-ray binaries because their temporal behavior closely resembles that of systems with Be companions (Bildsten et al. 1997). This paper reports the discovery and temporal behavior of the fourth member of this group, GRO J2058+42.

A 198 second periodic signal was observed in the BATSE data starting on 1995 September 14. At the same time a new source was also detected by Earth occultation measurements, which measure phase-averaged (total) flux. A location was determined from both the pulsed data and the non-pulsed data with a 95% confidence error box of about $4^\circ \times 1^\circ$ (Wilson et al. 1995). A *CGRO* target of opportunity was declared and the spacecraft was reoriented to allow scans of the region by the Oriented Scintillation Spectroscopy Experiment (OSSE), resulting in an improved $30' \times 60'$ (95% confidence) position (Grove 1995). The total flux peaked at about 300 mCrab (20-100 keV) and the pulsed flux (RMS deviation from mean) peaked at 140 mCrab (20-50 keV) on 1995 September 27. This bright outburst continued until 1995 October 30. A search of archival BATSE data from 1991 April until this bright outburst showed no previous outbursts.

An analysis of BATSE data following the bright outburst initially revealed three much weaker outbursts each lasting about two weeks with pulsed flux peaking at 15-20 mCrab (20-50 keV). These outbursts were spaced by about 110 days which allowed the peak of the next outburst to be predicted. A target of opportunity scan of the OSSE/BATSE error box was performed on 1996 November 28 with the *RXTE* Proportional Counter Array (PCA) yielding a 90% confidence $4'$ radius error circle centered on R.A. = $20^h 59^m.0$, Decl. = $+41^\circ 43'$ (Wilson, Strohmayer, & Chakrabarty 1996). BATSE also detected the source from 1996 November 23- December 1. Another outburst was detected by BATSE about 110 days later (1997 March 16-20.) Three shorter outbursts with peak pulsed fluxes of about 8 mCrab were detected by BATSE halfway between the first four 15-20 mCrab outbursts. The *RXTE* All-Sky Monitor detected all 8 weak outbursts with approximately equal durations and intensities. An archival search of *ROSAT* data found no sources within

the error circle (J. Greiner, 1997, private communication.) No optical counterpart has been found to date.

In this paper we present the BATSE and *RXTE* observations of GRO J2058+42. Our observations with BATSE include histories of pulse frequency and pulsed flux from 1995 September - 1997 March, a history of phase-averaged flux for the “giant” outburst (1995 September-October), and pulse profile variations dependent upon energy and outburst phase of the “giant” outburst. An *RXTE* PCA observation of a weak outburst on 1996 November 28 includes a fit to the scan data used to better locate GRO J2058+42 and pulse profiles. We compare BATSE and *RXTE* ASM observations of the 8 weak outbursts from 1995 December - 1997 March. We then discuss the implications of our results.

2. Observations and Analyses

BATSE consists of eight identical uncollimated detector modules positioned on the corners of the *CGRO* spacecraft such that the normal vectors of the detectors are perpendicular to the faces of a regular octahedron, providing all-sky coverage. The BATSE data presented here are taken with the large-area detectors (LADs), which are NaI(Tl) scintillation crystals with a geometric area of 2025 cm² and a thickness of 1.27 cm. The LADs are sensitive to photons from 20 to 1800 keV. Two BATSE data types were used in this analysis, the CONT (2.048 s, 16 energy channel) data and the DISCLA (1.024 s, 4 energy channel) data. A more complete description of the instrument and data types can be found in Fishman et al. (1989).

2.1. The Initial “Giant” Outburst

Figure 1 shows histories of spin frequency and pulsed intensity, determined by fits to 4-day intervals of the BATSE 20-50 keV DISCLA (1.024 second) data. Short intervals of data (200 s) were fit with a background model plus a sixth order Fourier expansion in the pulsed phase model to generate pulse profiles at the model frequency. (See Bildsten et al. 1997 for a detailed description of pulsed flux and pulsed frequency estimation techniques.) The pulsed phase model initially consisted of a constant frequency obtained from daily power spectra of the BATSE DISCLA data. The data were combined into 600 second intervals with continuous background models. For each four day span, the pulse profiles from the 600 s intervals were shifted in phase according to a range of trial frequency offsets from the pulse phase model (± 5 cycles day⁻¹). Then the profiles were summed for each

trial frequency offset. The best fit frequency was determined by the Z_6^2 test (Buccheri et al. 1983) which measured the significance of the first 6 Fourier amplitudes. The frequency estimates were iteratively improved by generating a new phase model from the best fit frequencies and repeating the process. For GRO J2058+42, root-mean-square (RMS) pulsed fluxes were estimated from the best fit pulse profile as

$$F_{\text{RMS}} = \left[\int_0^1 (F(\phi) - \bar{F})^2 d\phi \right]^{1/2} \quad (1)$$

where $F(\phi)$ is the pulse profile at phase ϕ , $0 \leq \phi \leq 1$, and $\bar{F} = \int_0^1 F(\phi) d\phi$ is the average flux. The pulsed fluxes in the bottom panel of figure 1 were determined at 4-day intervals, assuming an exponential energy spectrum,

$$f(E) = A \exp\left(-\frac{E}{E_{\text{fold}}}\right) \quad (2)$$

with a normalization A and e-folding energy $E_{\text{fold}} = 20$ keV.

For pulse periods longer than about 100 seconds, this frequency estimation method had an added complication if the pulse period was close to a harmonic of the spacecraft orbital period (≈ 93 min). The pulse period of GRO J2058+42 was close the 28th spacecraft orbital harmonic. Relatively bright sources produced intensity steps in the count rate in source-facing detectors upon entering or exiting Earth occultation. When the data from these detectors were fit for a range of frequencies that included a spacecraft orbital harmonic, the accumulated occultation steps produced a periodic signal which was sometimes more significant than the signal from GRO J2058+42. This effect was removed by discarding an interval of about 30 seconds of DISCLA data which was centered on the occultation step of each interfering source and by allowing a corresponding discontinuity in the background model. Occultations for the Crab and Cyg X-1 were always removed from the data. Also, occultations for GRS 1915+105, Sco X-1, and GRO J1744-28 were removed when they were bright.

From figure 1, which shows the determined pulse frequency and pulsed flux history of GRO J2058+42 from BATSE data, it is apparent that GRO J2058+42 experienced a large spin up during its initial 46 day outburst. The period changed by about 2 seconds across this outburst, corresponding to an average $P/|\dot{P}| \approx 12$ years. Measurements of the spin-up rate yielded a peak value of $(2.48 \pm .02) \times 10^{-11}$ Hz s $^{-1}$ (where we have neglected corrections for the pulsar’s orbital motion), which is comparable to peak spin-up rates seen by BATSE in “giant” outbursts from known Be transients (Bildsten et al. 1997). In the bottom panel of figure 1, the peak intensity of the initial outburst is about 10 times the peak intensity of later outbursts. The initial outburst begins at approximately the same orbital phase as

later outbursts, but peaks at a later phase. The large spin-up and brightness of the initial outburst compared to later outbursts leads us to classify it as a “giant” outburst (Stella, White, & Rosner 1986).

The total (pulsed+unpulsed) flux from GRO J2058+42 was determined using Earth occultation measurements. This technique measures the intensity of a known source by calculating the difference in total count rate in source-facing detectors just before and just after occultation by the Earth (Harmon et al. 1992). For sources with long pulse periods and large pulsed fractions, flux measurements from individual occultation edges can be biased by favoring a particular pulse phase. However, this bias was easily eliminated by averaging many occultation measurements to uniformly sample the pulse.

Both the Earth occultation measurements and the pulsed flux measurements were well fit by an exponential spectrum (see eq. 2) with E_{fold} values of 15-22 keV. No dependence of spectral shape on intensity was detected. The total 20-70 keV flux history for GRO J2058+42 was determined at 2-day intervals by fitting the Earth occultation count rates with equation (2) and assuming $E_{\text{fold}} = 20$ keV. This flux history is shown in figure 2. The weak outbursts were undetectable in Earth occultation data, with an upper limit of $\lesssim 50$ mCrab (3σ).

Pulse profiles for 4 day intervals were generated by epoch-folding BATSE CONT (2.048 s) data into 64 phase bins using a quadratic phase model (again neglecting the pulsar’s unknown orbit). Phase models were estimated at four day intervals by a grid search in frequency and frequency derivative, as described above. Each epoch-fold contained the usable data from a single spacecraft orbit. Data were excluded when the GRO J2058+42 was occulted and during intervals containing occultation steps for Crab and Cyg X-1. Gamma-ray bursts, Solar flares, South Atlantic Anomaly passages, and electron precipitation events in the data stream were also excluded.

We searched for pulse shape variations using a statistical comparison of pulse profiles formulated in the frequency domain. Wilson et al. (1997) show that the harmonic coefficients of a pulse profile are uncorrelated. For each single spacecraft orbit epoch-folded profile, these harmonic coefficients were calculated as

$$a_k = \frac{1}{N} \sum_{j=1}^N R_j e^{-i2\pi jk/N} \quad (3)$$

where k is the harmonic number, $i = (-1)^{1/2}$, $N = 64$, the number of phase bins in the pulse profile, and R_j is the count rate in the j th bin of the pulse profile. We calculated the mean value \bar{a}_k from the measurements of a_k from the epoch-folded profiles contained within each 4-day interval corresponding to the phase model. We calculated the error on

the mean $\sigma_{\bar{a}_k}$ from the sample variance of the measurements of a_k . By comparing signal power to noise power $\bar{a}_k^2/\sigma_{\bar{a}_k}^2$, we determined that only the first 6 harmonics were significant. The average noise level was higher than expected for Poisson counting noise because Cyg X-1 was nearly always present in the field of view and was in an active state during the giant outburst of GRO J2058+42, introducing spurious noise power over a broad range of frequencies. The observed noise power spectrum exhibited a turnover frequency consistent with Cyg X-1 (Crary et al. 1996). Noise from Cyg X-1 also affected the sensitivity of the frequency search.

We attempted to remove Cyg X-1 in the time domain by simultaneously fitting the two sources using different assumed spectra. For each phase bin, fluxes were determined for GRO J2058+42 and Cyg X-1 by minimizing

$$\chi^2 = \sum_{i=1}^6 \frac{(\Delta C_i - \alpha_i S - \beta_i N)^2}{\sigma_i^2} \quad (4)$$

where ΔC_i is the mean subtracted count rate for the i th energy channel in a 4-day mean profile, S is the GRO J2058+42 flux at 30 keV, and N is the Cyg X-1 flux at 30 keV. The parameter α_j is the assumed energy spectrum for GRO J2058+42, $f(E) = \exp(-(E - 30 \text{ keV})/20 \text{ keV})$, convolved with the detector response to yield the expected count rate in energy channel i . The parameter β_i was calculated in the same way using a photon power law spectrum with photon index -1.85 for Cyg X-1. The energy channel range used corresponded to 20-125 keV. GRO 2058+42 was detectable up to about 70 keV while Cyg X-1 emission was present up to about 400 keV. This method worked well for only the brightest profiles, due to statistical limitations. Figure 3 shows the fit to a profile from 1995 September 23-27 near the peak of the giant outburst. Noise from Cyg X-1 appears to be causing high frequency features in the profile.

Since noise from Cyg X-1 could not be directly removed, only the first 6 harmonics of the pulse profiles were retained for pulse shape analysis, thus avoiding most of the noise effects. Groups of harmonic limited 4-day profiles were phase-aligned and averaged to improve statistical significance. Mean profiles from different epochs were compared by minimizing

$$\chi^2 = \sum_{k=1}^6 \frac{|\bar{p}_k - \bar{t}_k \beta e^{2\pi i \Delta \phi}|^2}{\sigma_{\bar{p}_k}^2 + \beta^2 \sigma_{\bar{t}_k}^2} \quad (5)$$

where \bar{p}_k and \bar{t}_k were the harmonic coefficients of the first and second mean profiles respectively and $\sigma_{\bar{p}_k}$ and $\sigma_{\bar{t}_k}$ were the corresponding errors. The second mean profile was scaled by a factor β and shifted in phase by $\Delta \phi$ to obtain the best fit.

Phase aligned pulse profiles were thus constructed from BATSE 20-70 keV CONT data from four intervals: (a) 1995 September 11-18, (b) September 23-30, (c) October 5-17,

and (d) October 17-28. The intensity intervals used to construct these profiles are denoted by dotted lines in figure 2 and are labeled accordingly. The profiles themselves are shown in figure 4. Average count rates measured by Earth occultation for these time intervals were added to the profiles shown to demonstrate the relative intensities of the profiles. Errors on these count rates were not included in the errors plotted because the profile comparisons involved only the mean subtracted profiles. The peak-to-peak pulse fraction, $(\bar{r}_{\text{pulsed}} - r_{\text{pulsed}_{\text{min}}})/r_{\text{occ}}$, for these profiles was consistent with a constant value of 0.46 ± 0.02 .

The profiles near the peak of the outburst (figure 4b) were significantly different from profiles at lower intensities ($\lesssim 100$ mCrab). The main pulse appeared to evolve from a faster rise than fall to a slower rise than fall, although the primary differences in the profiles were occurring in the region between the large pulses (phase 0.5-1). Profile (a) was relatively flat in the interpulse region. The deep dip near phase 0.6 persisted in higher channels and was most likely due to Cyg X-1. Profile (b) slowly declined in intensity to a minimum near phase 0.7, after which it slowly increased in intensity. Profiles (c) and (d) both had a feature from phase 0.8-1.0 that did not persist at higher energies, so it was most likely intrinsic to the source. The profile in (a) was significantly different from the profile in (d), although the intensities were similar. However, profiles (c) and (d), both from the fall of the outburst were consistent with one another, although their intensities differed. Profiles during the rise of the outburst differed from those in the fall of the outburst which implies that the shape of the profile was dependent upon more than simply the mass accretion rate.

Next we compared profiles for the energy intervals 20-40 keV and 40-70 keV. We detected profile variations with energy as shown in figure 5. The profiles shown are from the brightest interval 1995 September 23-30. Comparisons from fainter intervals were also suggestive of energy dependent pulse shape variations. In figure 5, average count rates and errors from Earth occultation measurements were added to the profiles. The bottom panel is the hardness ratio given by

$$r = \frac{h + \Delta h}{s + \Delta s} \quad (6)$$

where h is the average count rate measured by Earth occultation for 40-70 keV, Δh is the mean subtracted pulse profile count rate for 40-70 keV, s is the average count rate for 20-40 keV, and Δs is the mean subtracted profile for 20-40 keV. The errors shown are the errors on the difference $r - h/s$, since we are interested in where the hardness ratio deviated from the mean value, 0.74 ± 0.06 . The hardness ratio demonstrated that the rise of the pulse (phase 0.0-0.25) had a harder spectrum than later pulse phases.

2.2. Location with *RXTE*

The Proportional Counter Array (PCA) on *RXTE* consists of five proportional counters sensitive to photons from 2-60 keV and has a total collecting area of 6500 cm². The PCA is a collimated instrument with an approximately circular collimator efficiency with a FWHM of about 1° (Jahoda et al. 1996). PCA observations of GRO J2058+42 were performed on 1996 November 28. A series of scanning observations was followed by a short (≈ 900 s) dwell on the source. A frequency consistent with the BATSE barycentered measurement, $\nu = 5.1153 \pm 0.0003 \times 10^{-3}$ Hz at MJD 10416, and three higher harmonics were clearly detected during the pointed observation. Figure 6 shows the pulse profiles as a function of energy from the PCA data. The pulse shape appears to be changing with energy. Evidence of variations can be seen by comparing the feature near phase 0.6 in different energy ranges. This feature is quite prominent at lower energies but is essentially nonexistent above 20 keV.

To estimate the position of GRO J2058+42 from the PCA scanning data, we analyzed the two largest scan peaks simultaneously. The relatively constant background during this time greatly simplified the analysis. We used the spacecraft pointing data combined with a model of the collimator response to calculate the contribution to the total 2-60 keV count rate from a constant (in time) background B and a model source of assumed constant intensity S (counts s⁻¹) located at celestial coordinates α , and δ . We minimized the four parameter function

$$\chi^2 = \sum_i \frac{(O_i - M_i(S, \alpha_j, \delta_j, B))^2}{\sigma_i^2}. \quad (7)$$

Here O_i , M_i are the observed and predicted count rates for time interval i , and σ_i^2 is the variance on the predicted count rate. The best-fit source position was that which had the minimum value for χ^2 . We determined a statistical confidence region from the appropriate value of $\Delta\chi^2$ for the 3 interesting parameters (S, α_j, δ_j .) To the extent that the background was flat the background parameter was not relevant to the determination of the confidence region (see Lampton, Margon, & Bowyer 1976). We show in figure 7 the data and best-fit model. The resulting best-fit position was $\alpha = 20^h59^m$, $\delta = 41^\circ43'$ (Wilson, Strohmayer, & Chakrabarty 1996). The total uncertainty in the position was not dominated by the statistical error, rather, time variability of the source as well as uncertainties in the collimator model contributed to the error budget as well. Our current understanding of these effects yielded a final circular confidence region (90 %) of radius 4' centered at the above position.

2.3. The Weak Outbursts

The *RXTE* All-Sky Monitor (ASM) consists of three wide-angle shadow cameras equipped with Xenon proportional counters with a total collecting area of 90 cm². The ASM provides 90 second snapshots of most of the sky every 96 minutes in three energy channels from 2-12 keV (Levine et al. 1996). Archival and new image data at the position of GRO J2058+42 determined by the PCA were searched by the *RXTE* ASM team and weak outbursts were detected. Single dwell (90 s time resolution) data during these outbursts were epoch-folded using phase models determined from BATSE data, but no pulsations were detected. Figure 8 is a comparison of the BATSE pulsed flux (20-50 keV) and the flux as measured by the *RXTE* ASM. The BATSE data indicated significant detections every ≈ 110 days of outbursts peaking at 15-20 mCrab (20-50 keV). Halfway between these outbursts BATSE detected shorter weaker outbursts with peak fluxes < 15 mCrab. The ASM data show outbursts every 54 days (Corbet, Peele, & Remillard 1997) that were all similar in intensity and duration. Figure 9 shows BATSE pulsed flux and ASM flux from the first 7 weak outbursts folded at a period of 110 days with epoch Julian Date 2450302. The folding epoch was chosen near the peak of a stronger outburst in the BATSE data. The outbursts near phase 0.0 were much brighter in the BATSE data than those near phase 0.5, while both outbursts were similar in the ASM data. No known systematic effects would remove or weaken outbursts in the BATSE data at 55 day intervals. A closer analysis of the individual *RXTE* ASM energy channels did not show a significant difference in the spectral hardness of the two sets of outbursts within the 2-12 keV band.

3. Discussion

The optically identified companions for transient pulsars with pulse periods longer than one second are all Be or Oe stars. Long term studies of these Be/X-ray binaries have demonstrated that giant outbursts followed by or interspersed with a series of periodic normal outbursts appear to be typical behavior for Be/X-ray binaries (Bildsten et al. 1997). GRO J2058+42 is most likely a Be/X-ray pulsar because it exhibits transient outbursts recurring with a presumed orbital period of 110 days and it has both giant and normal outbursts. An orbital period of 110 days places GRO J2058+42 along the orbital period spin period correlation for Be/X-ray binaries (Corbet 1986, Waters & van Kerkwijk 1989.)

The giant outburst of GRO J2058+42 showed enough dynamic range that we can use the relationship between torque and observed flux to test accretion theory. Simple accretion theory assumes that material from the companion star is flowing onto a rotating neutron star with a magnetic field. The magnetic field is so strong that it determines

the motion of the material in a region of space surrounding the neutron star called the magnetosphere. The size of this region, the magnetospheric radius r_m , is defined to be the distance from the neutron star at which all magnetic field lines are just closed loops. Another important length scale is the corotation radius, r_{co} , the distance from the neutron star where centrifugal forces just balance local gravity. If $r_m > r_{co}$, accretion is not expected to occur. Accretion theory predicts $r_m \propto \dot{M}^{-2/7}$ for $r_m < r_{co}$ for disk or wind accretion. The accretion torque N is given by $N \propto \dot{M} \sqrt{r_m}$. We can assume the bolometric flux F_{bol} is related to the mass accretion rate \dot{M} by $\dot{M} \propto F_{bol}$. Therefore, simple accretion theory predicts $\dot{\nu} \propto F_{bol}^{6/7}$, where $\dot{\nu}$ is the spin-up rate of the neutron star (Henrichs 1983 and references therein).

Figure 10 shows the observed 20-100 keV flux as measured by Earth occultation plotted versus the measured frequency derivative $\dot{\nu}$ during the giant outburst. The frequency derivatives were generated by a search performed on the BATSE DISCLA 20-50 keV data over a grid of trial frequencies and frequency derivatives. This technique was identical to that described in section 2.1 except that the pulse profiles were shifted according to a grid of frequency offsets and frequency derivatives, rather than only frequency offsets. The search yielded maximum spin-up rates of 5×10^{-12} Hz s⁻¹ in the weak outbursts. If we assume that the orbital contribution was small compared to the intrinsic $\dot{\nu}$, we can treat the measured $\dot{\nu}$ as equal to the intrinsic $\dot{\nu}$ and compare it to the total flux in the BATSE energy range. Clearly, $\dot{\nu}$ and the total flux were correlated, hence an accretion disk was likely to be present. The power law $\dot{\nu} \propto F_{obs}^\gamma$ with $\gamma = 6/7$, which is predicted by accretion torque theory, is shown in figure 10. Also shown is the best fit curve with $\gamma \simeq 1.2$. Orbital contributions to the torque and the fact that BATSE does not measure the bolometric flux may explain the discrepancy between the measured slope and accretion theory. Interestingly, a similar fit to EXOSAT data from the 1985 giant outburst of the Be/X-ray binary EXO 2030+375 also gave $\gamma \simeq 1.2$ (Reynolds et al. 1996).

In addition to testing accretion theory, we can use the maximum $\dot{\nu}$ ($\dot{\nu}_{max} = 2.48 \times 10^{-11}$ Hz s⁻¹) from the giant outburst to estimate a distance to GRO J2058+42. The luminosity is related to $\dot{\nu}$ by

$$L_{37} = 4.83 \times 10^{13} \mu_{30}^{-1/3} m^{1/2} R_6^{-1} I_{45}^{7/6} n(\omega_s)^{-7/6} \dot{\nu}^{7/6} \quad (8)$$

where the notation is $\mu_{30} = \mu/10^{30}$ G cm³, $m = M_x/M_\odot$, $R_6 = R/10^6$ cm, $I_{45} = I/10^{45}$ g cm², and $L_{37} = L_{acc}/10^{37}$ ergs s⁻¹. The neutron star has magnetic moment μ , radius R , mass M_x , moment of inertia I , accretion luminosity L_{acc} , and “dimensionless torque” $n(\omega_s)$. We assumed the very slow rotator case of $n(\omega_s) \approx 1.4$ (Henrichs 1983 and references therein). We used typical values ($m = 1.4$, $R_6 = 1$, $I_{45} = 1$). Since μ_{30} is less well known, we calculated bolometric luminosities, $L_{acc} \simeq 0.7 - 3.5 \times 10^{38}$ ergs s⁻¹, for the range

$\mu_{30} = 0.1 - 10$. These luminosities were comparable to the Eddington limit for neutron stars, $L_{\text{Edd}} \simeq 2 \times 10^{38}$ ergs s^{-1} . Next, to calculate the distance, we can use the 20-100 keV flux corresponding to $\dot{\nu}_{\text{max}}$, $F_{\text{max}} = 4.76 \times 10^{-9}$ ergs cm^{-2} s^{-1} . Lastly, we must calculate a bolometric correction α , the ratio between the BATSE flux and the total 2-100 keV flux. Simultaneous BATSE and *RXTE* measurements from 1996 November yielded a bolometric correction of $\alpha \simeq 0.4$. Then the distance d is given by

$$d = \frac{1}{3.09 \times 10^{21} \text{cm}} \left(\frac{\alpha L_{\text{acc}}}{4\pi F_{\text{max}}} \right)^{1/2} \text{kpc} \quad (9)$$

which gives distances of 7-16 kpc for GRO J2058+42. For these distances the estimated bolometric luminosity for the 1996 November outburst is $L_{\text{bol}} \simeq 0.2 - 1 \times 10^{37}$ ergs s^{-1} . Bolometric luminosities for the intermediate weaker outbursts (in the BATSE data) appear to be similar to the 1996 November outburst, but are more uncertain because complete spectral and pulsed fraction information are unavailable.

The weak outbursts provide interesting, but difficult to interpret, information about this system. The BATSE data indicate brighter and longer outbursts every ≈ 110 days with weaker outbursts in between, while the ASM data show outbursts every 54 days that are similar in intensity and duration (fig 8 & Corbet, Peele, & Remillard 1997). The intermediate weaker outbursts in the BATSE data must be of a different character than the stronger outbursts. The fact that BATSE detects a 110 day periodicity and *RXTE* detects a periodicity at half that period implies that either a spectral change or a change in the pulse fraction is occurring every other outburst, indicating a difference in accretion mode. An analysis of the three *RXTE* ASM energy bands shows that both sets of outbursts have comparable intensity in the 5 - 12 keV band. This implies that if a spectral change is occurring it is above 12 keV. The observed periodicity may be interpreted in two ways: (1) the 110 day cycle observed in the BATSE data is the orbital period and 2 outbursts are occurring each orbit; or (2) the orbital period is 54 days and the spectrum (or pulse fraction) alternates every other orbit for at least 9 orbits. We can find no plausible explanation for an alternating change in spectrum or pulse fraction that persists for at least 9 orbits if the outbursts are produced by periastron passage in a 54 day orbit. Therefore we interpret the observed 110 day periodicity as the orbital period.

We propose that GRO J2058+42 is undergoing periastron and apastron outbursts in a 110 day orbit. A neutron star in an inclined orbit combined with concentration of material in the equatorial plane of the Be star is a possible explanation for the outburst behavior observed in GRO J2058+42. The same velocity kicks that produce an eccentric orbit could also produce an inclined orbit. Outbursts would occur twice per orbit when the neutron star crosses the equatorial plane of the companion (Priedhorsky & Holt 1987). From the BATSE data, we measured the separation between the brighter outbursts to be 110 ± 3

days and the separation between brighter and weaker outbursts to be $\Delta T = 54.5 \pm 2.3$ days. If we assume the separation between the brighter outbursts is the orbital period, P_{orb} , then $\Delta T/P_{\text{orb}}$ falls in the 95% confidence interval $0.45 < \Delta T/P_{\text{orb}} < 0.55$. For this interval the separation between periastron and the line where the neutron star's orbit intersects the equatorial plane of the companion is $\nu < 12.1^\circ$ for a typical eccentricity, $e = 0.35$. Hence this mechanism would produce outbursts near periastron and near apastron. This mechanism does not, however, explain the intensity differences seen only in the higher energies (20-50 keV). Although an inclined orbit has often been proposed as a mechanism for outbursts in Be/X-ray binaries, two outbursts per orbit have not been seen in other Be/X-ray binaries to date. However, such behavior has been observed in wind-fed systems such as GX 301-2 (Koh et al. 1997).

Another explanation which does not require an inclined orbit suggests that two different accretion mechanisms could be at work in this system. An accretion disk is likely to be present during giant outbursts. Its presence helps to explain the large and steady spin-up rates seen during giant outbursts. A peak spin-up rate of $2.5 \times 10^{-11} \text{ Hz s}^{-1}$ was observed in GRO J2058+42. Bildsten et al. (1997) suggest that an accretion disk could remain after a giant outburst. Then normal outbursts could be produced by large tidal torques on the accretion disk during periastron passage. This could explain the series of normal outbursts following the giant outburst. The apastron outbursts could be produced by accretion from the equatorial outflow from the Be star. A slow dense outflow could produce outbursts at apastron (Waters et al. 1989). The two outbursts per orbit would be produced by different accretion mechanisms which could produce differences in spectra or in pulse fraction. Clearly, additional observations are needed to fully understand this source.

The quick-look ASM data on GRO J2058+42 were provided by the *RXTE*/ASM team at MIT and NASA/Goddard Space Flight Center. We thank Jan van Paradijs and Matthew Scott for helpful discussions. D. C. was a NASA Compton Postdoctoral Fellowship under grant NAG 5-3109. We thank the referee L. B. F. (Rens) Waters for helpful comments.

REFERENCES

- Bildsten, L. et al. 1997, *ApJS*, 113, 367
Buccheri, R. et al. 1983, *A&A*, 128, 245
Corbet, R. H. D. 1986, *MNRAS*, 220, 1047
Corbet, R., Peele, A., & Remillard, R. 1997, *IAU Circ.*, No. 6556

- Crary, D. J. et al. 1996, *A &AS*, 120, 153
- Fishman, G. J., et al. 1989, in *Proc. GRO Science Workshop*, ed. W. N. Johnson (Greenbelt:NASA/GSFC), 2
- Grove, J. E. 1995, *IAU Circ.*, No 6239
- Harmon, B. A., et al. 1992, in *Compton Observatory Science Workshop*, ed. C. R. Schrader, N. Gehrels, & B. Denis, *NASA Conf. Publ.* 3137, 69
- Henrichs, H. F. in *Accretion-Driven Stellar X-ray Sources*, eds. Walter H. G. Lewin & Edward P. J. Van Den Heuvel, 1983, New York: Cambridge University Press, 411
- Jahoda, K., Swank, J. H., Giles, A. B., Stark, M. J., Strohmayer, T. E., Zhang, W. & Morgan, E. H. 1996, *EUV, X-ray, and Gamma-ray Instrumentation for Space Astronomy VII*, ed. O. H. W. Siegmund & M. A. Grummin, *SPIE* 2808, 59
- Koh, D. T. et al. 1997, *ApJ*, 479, 933
- Lampton, M., Margon, B., & Bowyer, S. 1976, *ApJ*, 208, 177
- Levine, A.M., Bradt, H., Cui, W., Jernigan, J.G., Morgan, E.H., Remillard, R., Shirey, R.E., & Smith, D.A. 1996, *ApJ*, 469, L33
- Priedhorsky, W. C. & Holt, S. S. 1987, *Space Science Reviews*, 45, 291
- Reynolds, A. P. et al. 1996, *A&A*, 312, 872
- Stella, L., White, N. E., & Rosner, R. 1986, *ApJ*, 308, 669
- Waters, L. B. F. M. & van Kerkwijk, M. H. 1989, *A&A*, 223, 196
- Waters, L. B. F. M., de Martino, D., Habets, G. M. H. J., & Taylor, A. R. 1989, *A&A*, 223, 207
- Wilson, C. A. et al., 1995, *IAU Circ.*, No. 6238
- Wilson, C. A. et al. 1997, *ApJ*, 479, 388
- Wilson, C. A., Strohmayer, T., & Chakrabarty, D. 1996, *IAU Circ.*, No 6514

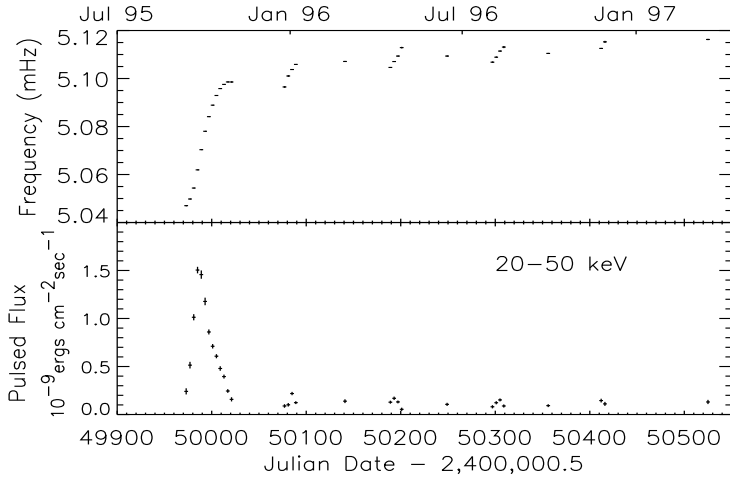


Fig. 1.— GRO J2058+42 spin frequency and pulsed flux measurements from BATSE. The frequencies were determined at 4-day intervals from 20-50 keV DISCLA data. The spin frequencies were barycentered, but have not been orbitally corrected since the orbit is unknown. Orbital effects are likely to be a substantial part of the observed spin-up (or down) during and between the weak outbursts. The pulsed fluxes were determined at 4-day intervals by assuming an exponential spectrum (see eq. 2) with an e-folding energy of 20 keV. Upper limits on the pulsed flux are not shown.

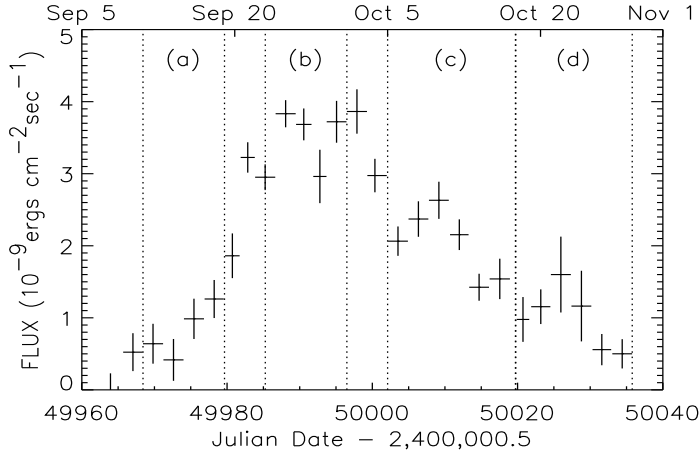


Fig. 2.— GRO J2058+42 total 20-70 keV flux as measured by Earth occultation. The fluxes were determined at 2-day intervals by assuming an exponential spectrum with an e-folding energy of 20 keV. The weak outbursts were not detected in Earth occultation data. The $3\text{-}\sigma$ upper limit on the peak fluxes for a 4-day interval was ≈ 50 mCrab. The labels (a),(b),(c), and (d) and dotted lines denote the intensity intervals used for the pulse profiles in figure 4.

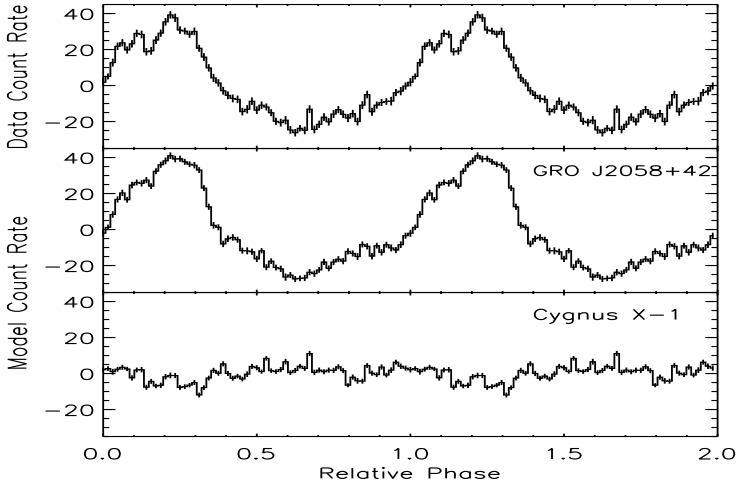


Fig. 3.— Noise effects in the GRO J2058+42 pulse profile produced by Cygnus X-1. The top panel is the epoch-folded 20-70 keV pulse profile for 1995 September 23-27. The center panel is the modeled count rate for GRO J2058+42, assuming an exponential spectrum (see eq. 2) with an e-folding energy of 20 keV. The bottom panel is the modeled count rate for Cygnus X-1 with a power law spectrum of photon index of -1.85. The count rate from Cygnus X-1 averaged near zero because we measured only the effects of noise from Cygnus X-1 on the mean subtracted profile.

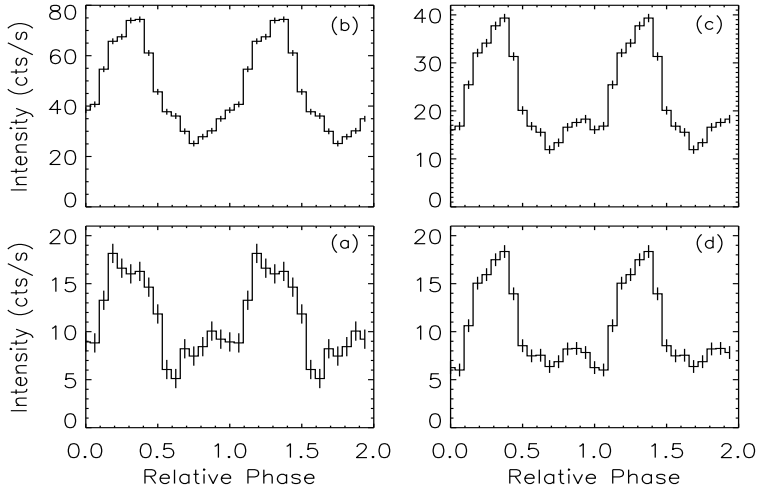


Fig. 4.— Phase aligned pulse profiles from 20-70 keV BATSE CONT data for the 4 intervals, (a) 1995 September 11-18, (b) September 23-30, (c) October 5-17, and (d) October 17-28. The average count rate from BATSE Earth occultation data from corresponding time intervals (figure 2) was added to the count rate plotted to demonstrate the pulsed fraction and relative intensity of the profiles, but was not been in the errors. The outburst proceeds clockwise from lower left.

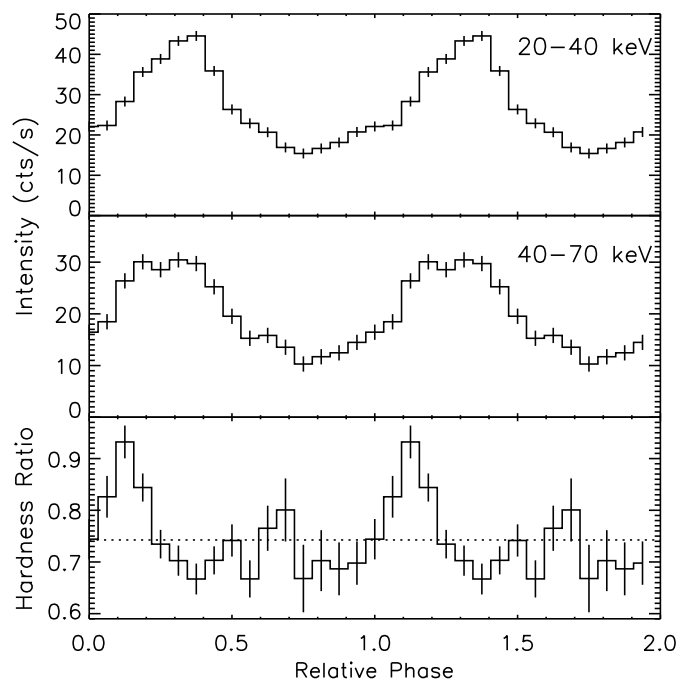


Fig. 5.— Energy dependent pulse profile variations for 1995 September 23-30. The top and center panels are the pulse profiles from 20-40 keV and 40-70 keV generated by epoch-folding BATSE CONT data. Average count rates and errors from the corresponding Earth occultation data were added to the epoch-folded profiles. The bottom panel is the ratio of the intensity in the center panel to the top panel. Errors are for the difference between this ratio and the average hardness ratio. The dotted line corresponds to the average hardness ratio, 0.74 ± 0.06 , calculated from Earth occultation data only.

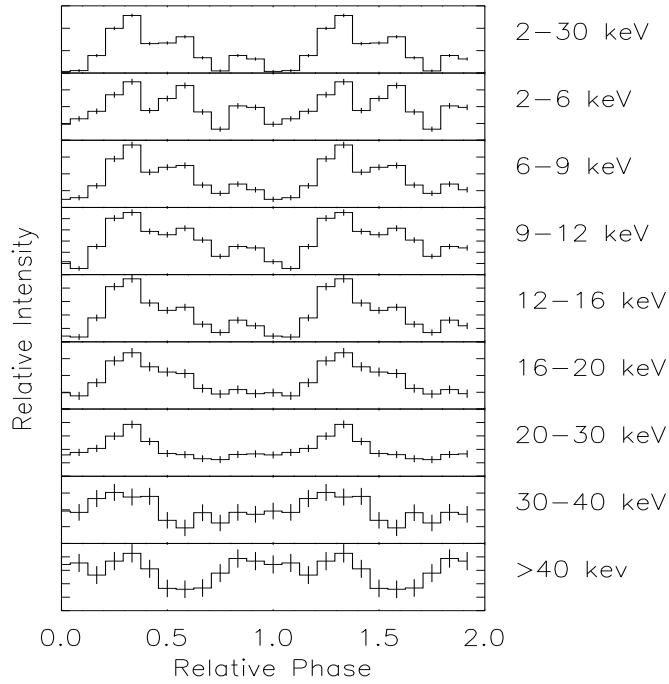


Fig. 6.— Pulse profiles from the pointed portion of the *RXTE* PCA observation on 1996 November 28. The pulse shape appears to be changing with energy.

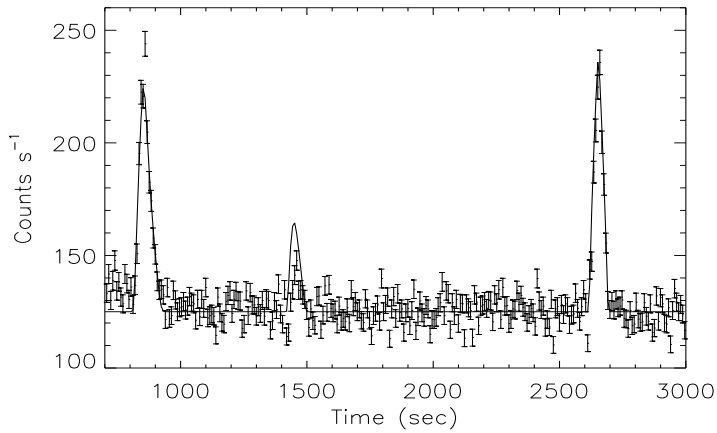


Fig. 7.— The observed count rate and best fit model for the scan portion of the *RXTE* PCA observation used to derive the position of GRO J2058+42. The peaks result from scans over and/or near the position of GRO J2058+42.

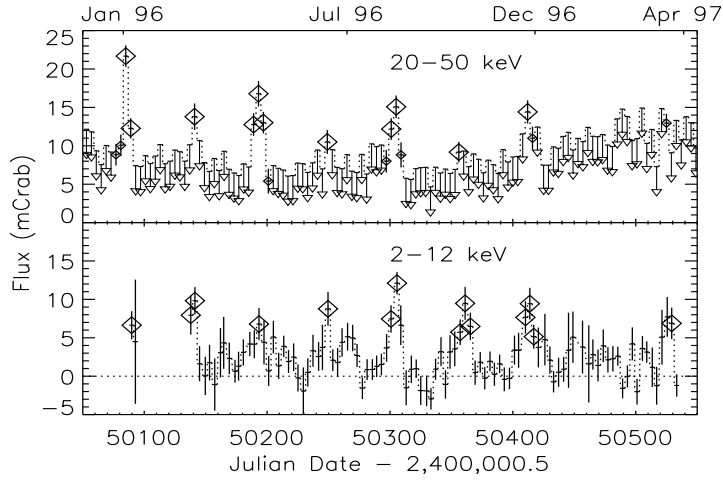


Fig. 8.— The top panel is BATSE (20-50 keV) pulsed flux where $1 \text{ mCrab} = 6.3 \times 10^{-3} \text{ keV cm}^{-2} \text{ s}^{-1}$. The large diamonds denote detections at the 99.9% confidence level. The small diamonds denote less significant measurements that are considered likely detections because the measured frequencies are well aligned with those that meet the 99.9% criterion. The likely detection for 1997 March 16-20 was confirmed by a more sensitive search in frequency and frequency derivative. Arrows denote 99% upper limits for the pulsed flux. The reduction in sensitivity from 1996 December is due to increased noise from Cygnus X-1. The bottom panel is the total flux as measured by the *RXTE* ASM (2-12 keV) where $1 \text{ mCrab} = 0.075 \text{ counts s}^{-1}$. The *RXTE* ASM flux has been binned into 4-day intervals. Points in the *RXTE* dataset where the count rate is at least 3 times the error are marked with large diamonds.

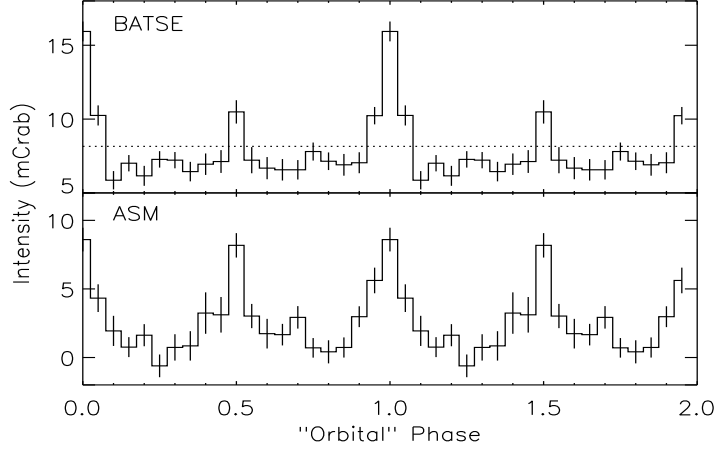


Fig. 9.— The BATSE (20-50 keV) pulsed flux and the ASM flux from the first 7 weak outbursts were epoch-folded at a period of 110 days (epoch Julian Date 2450302). The eighth outburst was excluded because noise from Cyg X-1 affected the BATSE measurements. The average 99% confidence upper limit on the BATSE pulsed flux is denoted by a dotted line.

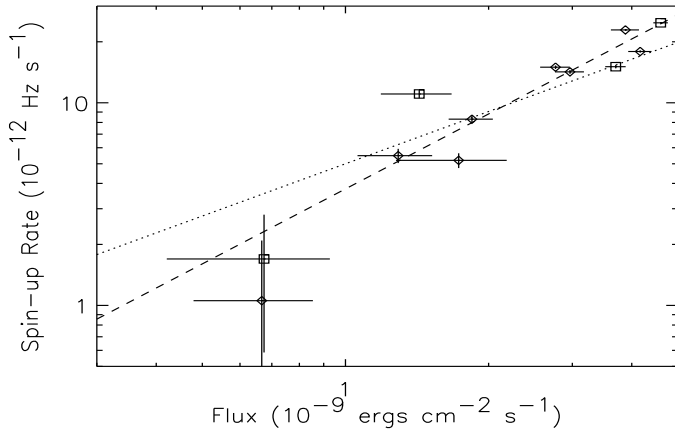


Fig. 10.— The observed 20-100 keV flux as measured by BATSE Earth occultation is plotted versus the measured pulsar spin-up rate $\dot{\nu}$ during the giant outburst. The square symbols indicate the rise of the outburst and the diamond symbols denote the decline. The dotted curve is a power law with an index of 6/7, the relationship between total flux and $\dot{\nu}$ predicted by accretion torque theory. The dashed curve is the best fit power law with an index of 1.2. The weak outbursts place an upper limit of $5 \times 10^{-12} \text{ Hz s}^{-1}$ on the orbital contribution to $\dot{\nu}$.